MEASUREMENT AND PREDICTION OF FULL SCALE ANNULAR SEAL COEFFICIENTS

by

Stefan Florjancic

Senior Field Engineer

Sulzer Bingham Pumps, Incorporated

Portland, Oregon

and

Thomas McCloskey

Manager, Steam Turbines and Auxiliaries

Electric Power Research Institute

Palo Alto, California

Stefan Florjancic graduated in 1982 from the Federal Institute of Technology in Zurich, Switzerland, with a degree in Mechanical Engineering. After training periods in pump factories in Switzerland, West Germany, U.S.A., France, and Brazil, he joined Sulzer Brothers Limited, Switzerland in 1983, and worked seven years in the area of mechanical development and design of pumps, mainly covering rotordynamic calculations and research.

Dr. Florjancic received his Ph.D. degree for a combined experimental and theoretical research thesis covering the rotordynamic influence of annular seals from the Federal Institute of Technology in Zurich in 1990. Subsequently, he joined Sulzer Bingham Pumps, Incorporated, Portland Oregon, where he currently works as a Senior Field Engineer. His responsibilities include general vibration acquisition and analysis, troubleshooting of pump installations, and rotordynamic and mechanical advising for pump designs.

Thomas H. McCloskey, is the Manager for Steam Turbines and Related Auxiliaries in the Rotating Machinery Program, Generation and Storage Division, for the Electric Power Research Institute (EPRI) in Palo Alto, California. Mr. McCloskey's responsibilities include the planning, management, and technology transfer of research and development projects relating to the thermal performance, availability, and life assessment of steam turbines, pumps, and related auxiliaries.

Mr. McCloskey has over 20 years experience in the design, operation, maintenance, and troubleshooting of steam turbines, pumps, and related auxiliaries and holds six patents in mechanical engineering.

Mr. McCloskey was the recipient of the ASME/EEI prime movers award for best technical paper in 1984. He is an author of over 30 technical papers on power plant equipment and in particular steam turbine generator and pump availability, life assessment, and thermal performance improvements.

ABSTRACT

The accurate prediction of rotordynamic behavior of centrifugal pumps has increased in importance over the last decade, with a steady increase in speed and power concentration. Designing a pump which has acceptable vibration characteristics when new is not sufficient. As various publications indicate, it is mainly wear of internal pump annular seals which lead to vibration problems of originally smooth running units [1, 2, 3, 4, 5, 6]. The calculation of pump vibrational behavior is an important element in establishing maintenance intervals to ensure reliable operation. While the mechanical rotor system and boundary conditions at journal bearings can be modelled quite accurately, interaction forces within the hydraulic part of the pump are not well known.

Impeller interaction is one important influence on rotordynamics. However, these forces are not sensitive to internal wear. Impeller interaction is treated by several authors [7, 8, 9]. Reliable dynamic modelling of annular seals is established within centrifugal pumps. Measured results of a full scale test machine are presented and used to confirm the newly developed, improved model. The overall influence of a change in seal design from smooth to serrated is shown. Additionally, it is demonstrated why the effect of wear deteriorates vibrational behavior and leads to the requirement of periodic internal seal replacement.

INTRODUCTION

The influence of annular seals in high energy centrifugal pumps on the rotordynamic behavior has been shown in many publications [1, 2, 3, 4, 5, 6]. Changes in seal configurations may alter the vibration levels of a pump. The flow resistance, and hence, the efficiency, also depend on the seal configuration. Rotordynamic problems generally become apparent only after some period of operation, when the seals have worn out. The design may be the cause of the vibrational problems. However, inadequate maintenance, i.e., inadequate machine handling leading to premature wear due to rub or abrasion, or excessive replacement intervals may as well be the primary cause of the problem.

Literature indicates that the wear of annular seals gradually reduces the pump critical speeds and, more importantly, decreases rotor damping, i.e., its capability to attenuate any kind of rotor vibrations. The example of Pace [1] indicates the drop of the first bending resonant frequency of a four stage boiler feed pump rotor from about 90 percent of running frequency in new

conditions to approximately 77 percent of running frequency with annular seals opened deliberately to twice the original clearance. However, most significant in this case was the reduction of the damping capability of the seals. The result was almost zero rotor damping, which leads to high vibrations and, with further wear, may eventually cause a catastrophic failure of the rotor system. A second example showing wear related rotordynamic instability is given by Valantas and Bolleter [4]. The five stage injection pump exhibited excessive wear after a short period of operation due to the high content of abrasives in the produced water. It was shown, that the resonant frequency drops from about 95 percent of running frequency with annular seals in original conditions to approximately 91 percent of running frequency with the excessively large seal clearances. Again, most important was the resulting loss of machine damping, leading the pump into instability manifested by dramatically high vibration levels at the subsynchronous resonant frequency.

The accurate knowledge of seal characteristics is very important. This knowledge establishes the basis for design improvements and for the prediction of appropriate maintenance intervals, with respect to internal wear. Therefore, rotordynamic and hydraulic characteristics of three full scale seal configurations were investigated in a new test machine, working at Reynolds numbers typically encountered in modern boiler feed pumps. The behavior of a smooth seal in new conditions, and a serrated seal in new and worn conditions was investigated [10] to determine the influences of design changes and wear.

The basic physical mechanisms which result in the rotordynamic influence of an annular seal are briefly explained. A new three volume theory based on bulk flow to solve for the rotordynamic effects is presented. The new theory and a previous state-of-the-art code are compared with the measured examples. This is a significant improvement over the previous theory which needs the seal friction behavior as input. The new theory can calculate rotordynamic and hydraulic coefficients of smooth and serrated seals without any additional information and with improved accuracy.

DESCRIPTION OF INTERACTION FORCES

In general the boundary conditions on rotors are described by two vibration frequency dependent forces, perpendicular to each other and the rotor centerline. These interaction forces are described by stiffness, damping, and mass or inertial terms which are proportional to vibration displacement, frequency, and frequency square, respectively. Cross coupled terms are needed to provide the interaction between the two perpendicular force directions, i.e., a displacement in the x direction can produce a force in the y direction. For the rotationally-symmetric annular seals the following matrix equation results. The main coefficients are equal and the cross coupled coefficients are equal in magnitude and opposite in sign, i.e., skew symmetric (journal bearings are normally not rotationally symmetric and hence, have full 2×2 matrices):

$$-\begin{bmatrix} F_x \\ F_y \end{bmatrix} \equiv \underbrace{\begin{bmatrix} K & k_c \\ -k_c & K \end{bmatrix}}_{\text{Stiffness}} \cdot \begin{bmatrix} X \\ Y \end{bmatrix} + \underbrace{\begin{bmatrix} C & c_c \\ -c_c & C \end{bmatrix}}_{\text{Damping}} \cdot \begin{bmatrix} \dot{X} \\ \dot{Y} \end{bmatrix} + \underbrace{\begin{bmatrix} M & m_c \\ -m_c & M \end{bmatrix}}_{\text{Mass}} \cdot \begin{bmatrix} \ddot{X} \\ \ddot{Y} \end{bmatrix} \quad (1)$$

In the plane of the seal, X and Y denote the displacements. The first and second time derivatives, the velocity and acceleration, are proportional to the vibration frequency and its square, respectively.

There is no a priori knowledge that this mathematical model matches the physical reality. However, measured results from various test programs have confirmed the approach to be appropriate.

TEST EQUIPMENT

Test Machine

The test machine, as given in Figure 1, is described in detail in [10], in an overview in [11], and is derived from the machine of [8]. The rotor is supported in a swinging frame allowing for linear vibration amplitudes in the vertical direction induced by the hydraulic shaker. From the entrance annulus, the fluid flows radially inwards across the controllable guide vanes, and through the narrow annular gap, formed by the seal insert and the rotor. Proximity probes measure actual rotor movement in radial direction. The rotor is attached directly to a calibrated piece of shaft, which is instrumented with strain gauges to measure the reaction forces on the vibrating rotor. Internal pressures and temperature as well as the flow downstream of the test machine were measured to monitor operating conditions including inlet swirl. Test configurations as measured are shown in Figure 2.

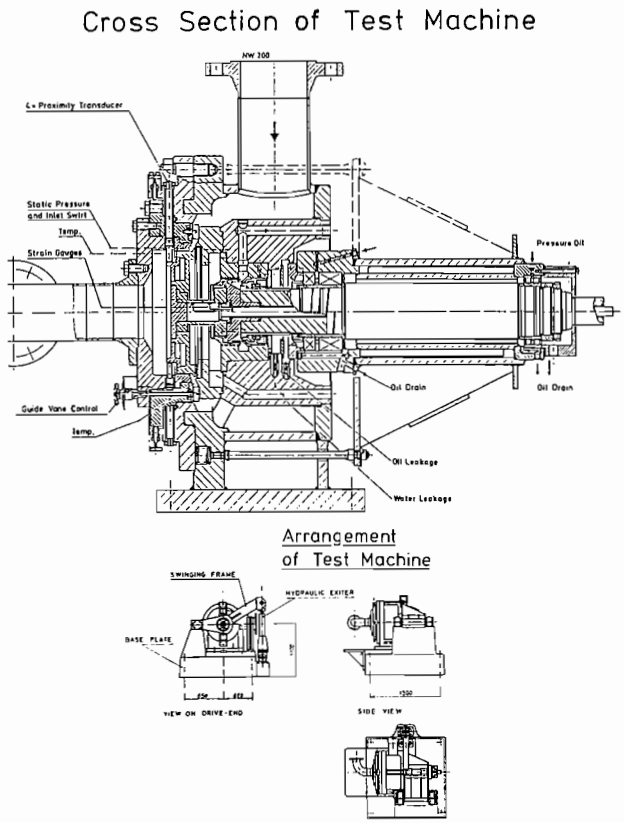

Figure 1. Test Machine for Annular Seals.

Static and dynamic properties of the test machine were calculated and optimized. Finite element method analysis and measurement of the machine showed no critical modes up to twice the measurement frequency range, and no misalignment or taper of the seal under operating pressure and temperature conditions.

Test Loop

The test loop is designed for demineralized water at a maximum temperature of 160°C (320°F). Pressure is generated in a standard pump, reaching a maximum of about 70 bar (1015 psi).

Geo-metry	Seal type	Surface	Gap width	Inlet swirl	Tempe-rature	Sketch
00S	straight	plain N8/N8	2.11 ‰	0.25 + Variation at 4 Points	40/70/160	
04S	straight	serrated N8/N8	2.11 ‰	0.15 + Variation at 4 Points	40/70/160	
04D	straight	serrated N8/N8	4.23 ‰	0.15 + Variation at 4 Points	40/70/160	

Definition of surface roughness acc. ISO 1302-1926

VSM 10231	Maximum allowable Surface roughness [1E-6 m]
N9	6,3
N8	3,2
N7	1,6
N6	0,8

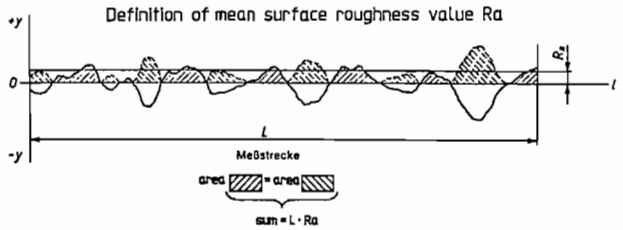

Figure 2. Measured Annular Seal Configurations and Definition of Surface Roughness.

Entrance pressure and flowrate to the test machine can be varied independently by valves in the main and the by pass branch. The return flow passes partially through the main heat exchanger, depending on the duty point.

Data Acquisition

Referring to Equation (1), there are basically two forces which are measured, and six unknown coefficients that are to be determined. Varying the excitation frequency of the hydraulic shaker results in varying time derivatives. Hence, a rapid frequency sweep, i.e., changing the frequency of the sinusoidal shaker input rapidly from 10 to some 120 percent of rotating frequency, yields the frequency-dependent interaction forces, and a least square fit determines the rotordynamic coefficients.

The force and displacement signal flow are shown in Figure 3. The signal wires of the dynamometer are led through the shaft, the coupling and the gear box into the rotating amplifier, to permit the slip ring assembly to transmit the information without loss. Radial displacement is measured in both horizontal and vertical direction. In the subsequent data processing, all signals are averaged after the analog digital conversion. The curve fitting of the frequency dependent force displacement relation finally yields one reliable set of stiffness, damping, and mass coefficients.

The signal flow for operating conditions is indicated in Figure 4. Fluid temperatures in front and behind the seal are measured. The pressure of individual locations is measured with strain-gauge type transducers, located outside of the machine. The frequency of the turbine flowmeter and the measured rotating frequency of the shaft, are the only data to be entered manually.

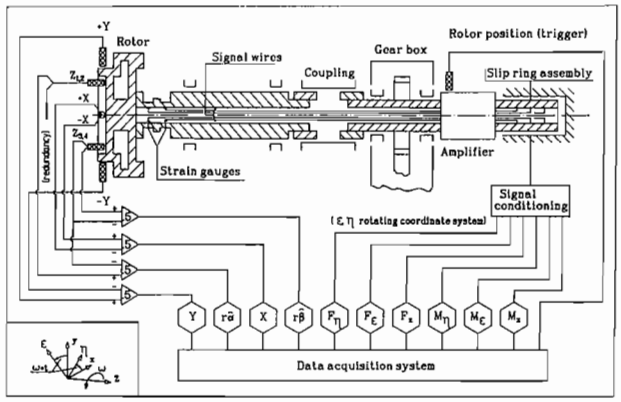

Figure 3. Measurement of Displacement and Force, Signal Flow.

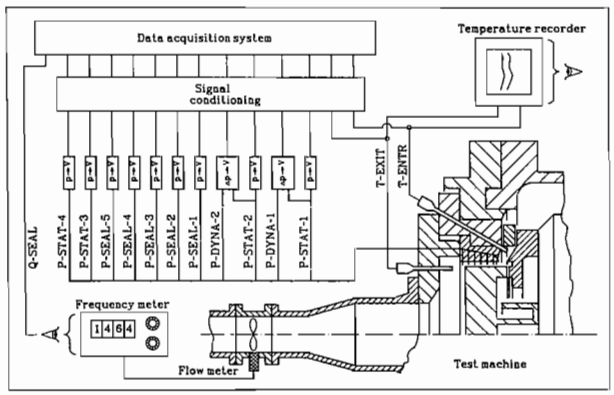

Figure 4. Measurement of Operating Conditions, Signal Flow.

With knowledge of the geometry, all essential operating conditions including fluid properties, can be derived:

- Rotor speed
- Density, viscosity (from temperature)
- Mean pressure drop
- Inlet swirl (from velocity head at pitot)
- Mean meridional velocity
- Friction coefficient (static pressure distribution within seal)

This information can than be used to normalize measured rotordynamic and hydraulic coefficients present *vs* Reynolds numbers.

Measuring Range

To establish the desired range of test parameters, operating conditions for an annular seal in a centrifugal pump were carefully considered. Within certain limits, the pressure generated in an impeller is approximately proportional to the square of the rotor speed. The axial leakage velocity v across an annular seal is approximately proportional to the square root of the pressure generated in the according impeller. Hence, the leakage velocity is approximately proportional to the rotor speed. Since the axial and circumferential Reynolds numbers are defined in terms of the axial leakage velocity and the circumferential seal surface velocity, respectively (see NOMENCLATURE), the ratio of these two dimensionless numbers is about constant for a specific impeller:

$$\frac{Re_a}{Re_c} = \frac{v}{\text{omega} \cdot R} = 0.45 \text{ to } 0.95 \qquad (2)$$

The geometric dimensions of the seal are directly correlated to the outer diameter, D_2, of the impeller. D_2 is a principal factor which determines the pressure generated at a certain speed; hence, the scale of the pump cannot change the ratio of Equation (2). The ratio of the two Reynolds numbers must lie in the narrow range shown in (2) for specific speeds typically used in boiler feed pumps. The ratio will be lower for very high specific speed impellers.

With this insight, the measuring range can be defined as shown in Figure 5. Axial and circumferential Reynolds numbers were selected at three fixed ratios: 0.3, 0.6 and 0.9 and range up to some 220,000 and 280,000, respectively. The large range was attained by varying temperatures from 20°C (68°F) to 160°C (320°F) as shown in Figure 6.

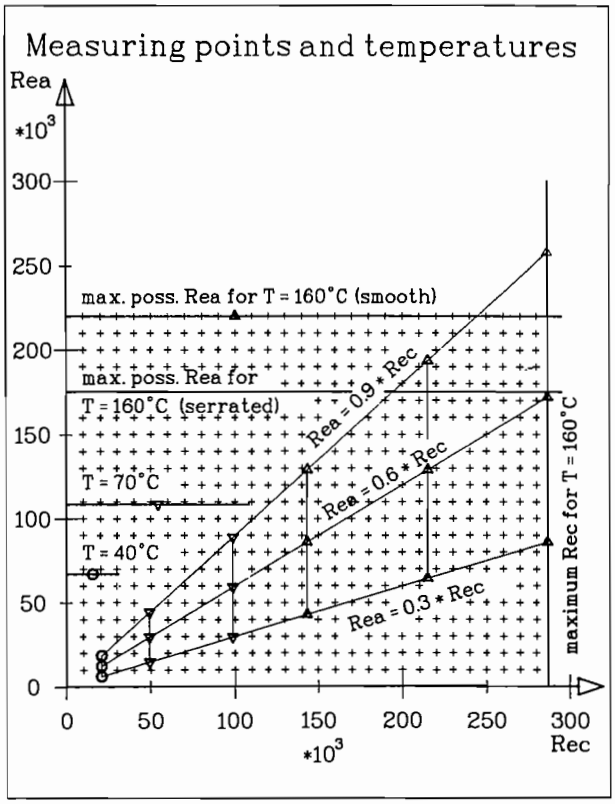

Figure 5. Nondimensional Test Operating Conditions.

Inlet Swirl

Water exiting an impeller and flowing radially inwards between the impeller shroud and the casing reaches a nondimensional inlet swirl U_{th0} of about 0.7 ÷ 0.8 at a wear ring entrance. With the adjustable vanes, a maximum of about U_{th0} = 0.15 could be reached over the whole Re_a range. To get detailed information about the influence of inlet swirl on coefficients, a variation from negative to maximum positive prerotations was measured. The information was used to extrapolate the coefficients to more realistic inlet swirls (Figure 7).

Test Program

Results of a smooth seal and a serrated seal with nominal and twice nominal clearance (see Figure 2) are presented. The

Seal diameter:	350	mm	13.78	in
stepped:	350/325	mm	13.8/12.8	in
Radial clearance:	0.37	mm	0.015	in
double:	0.74	mm	0.03	in
Seal length:	40	mm	1.57	in
Water temperature:	20/70/80/160	°C	68/158/176/320	°F
Max. pump speed:	4000	rpm		
Max. pressure difference:	appr. 60	bar	870	p.s.i.
Max. circumf. Re-number:	275'000	[-]		
Max. axial Re-number:	175'000 (rough) 225'000 (smooth)			

TYPICAL VALUES FOR BFP'S:

Re_a / Re_c = 0.4 to 0.9 (measured 0,3 ; 0,6 & 0,9)

Re_c = 200'000 to 260'000

Re_a = 100'000 to 150'000

Figure 6. General Test Parameters versus Typical Values.

nominal relative seal clearance (clearance to radius ratio) varies generally from about 0.15 to 0.3 percent, depending on the size and the application of the pump. The clearance is assumed to double for "worn condition." The wear ring diameter tested corresponds approximately to an impeller diameter $D_2 \approx 500$ mm (19.7 in). Note the definition of the surface roughness in Figure 2; each step increases the roughness by a factor of two.

For presentation, normalized coefficients are formulated using the pressure differential, the radius, the seal clearance, the length and, partially, the angular rotor speed:

$$F_r^*, F_t^* = \frac{(F_r, F_t)/e \cdot h_0}{L_{Seal} \cdot R \cdot dp} \qquad K^*, k_c^* = \frac{(K, k_c) \cdot h_0}{L_{Seal} \cdot R \cdot dp}$$

$$C^*, c_c^* = \frac{(C, c_c) \cdot h_0 \cdot \text{omega}}{L_{Seal} \cdot R \cdot dp} \qquad M^*, m_c^* = \frac{(M, m_c) \cdot h_0 \cdot \text{omega}^2}{L_{Seal} \cdot R \cdot dp} \qquad (3)$$

Experience with measured data revealed that normalized rotordynamic coefficients become constant at constant Re_a to Re_c ratios. Hence, the huge amount of information could be condensed by plotting the mean values as bar charts for individual Re ratios.

Vibration frequency dependent radial and tangential forces are only plotted at one selected ratio of excitation to running frequency, 0.8. Typical ratios for instabilities at high energy pumps range from about 0.7 to 0.9 [1, 2, 3, 4, 5, 6].

MEASURED DATA

A detailed error estimation can be found in [10] and [11], where the following worst-case uncertainties of nondimensional rotordynamic coefficients were established:

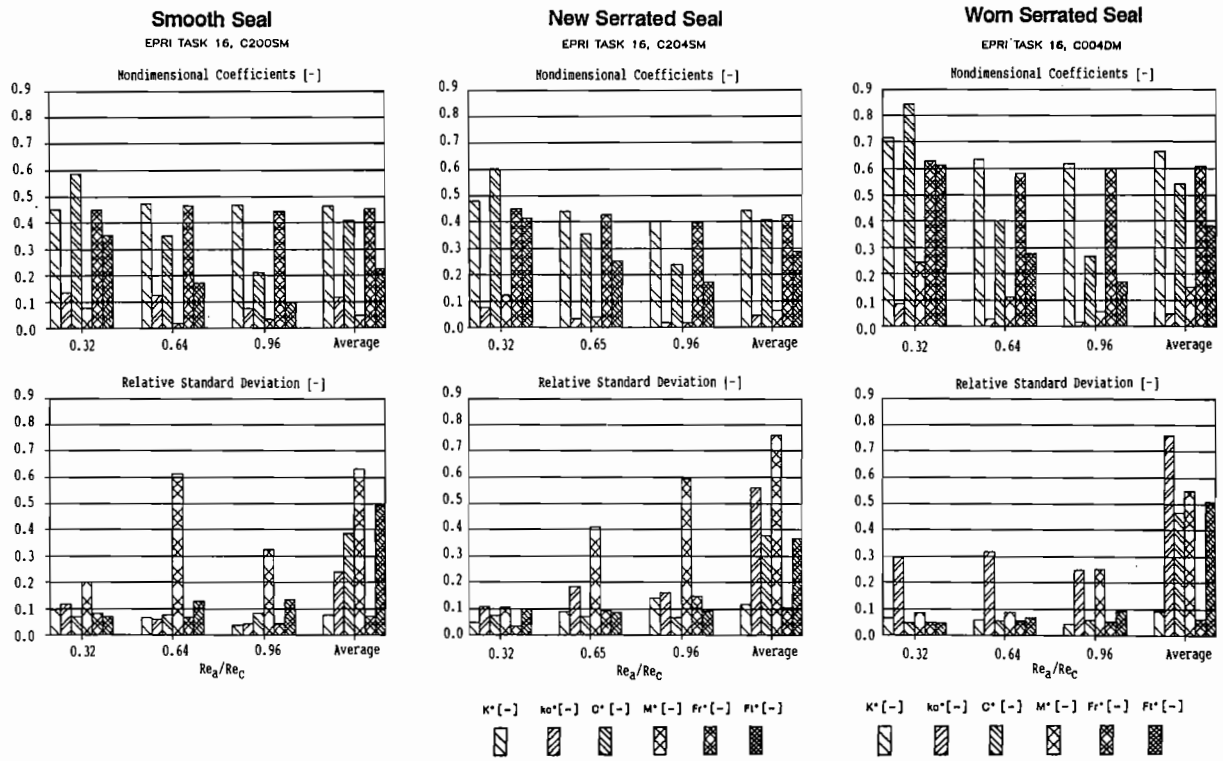

Figure 7. The Influence of Inlet Swirl on Rotordynamic Coefficients.

K*: ≈ ± 13 %	k_c*: ≈ ± 16 %
C*: ≈ ± 13 %	c_c*: ≈ ± 41 %
M*: ≈ ± 14 % (min.)	m_c*: ≈ ± 115 %
M*: ≈ ± 21 % (mean Re-ratio)	
M*: ≈ ± 56 % (max.)	

Only the two stiffness coefficients, the direct damping, and the direct mass term at smallest Re ratios are reliable results. However, large relative errors occur only for coefficients with absolute magnitudes too small to have any significance.

Discussion of Rotordynamic Coefficients (Figure 8)

00S

The normalized direct stiffness of the smooth seal exhibits scatter (relative standard deviation) well within the limits of measurement errors and is constant for all Re ratios.

The cross coupled stiffness, which depends strongly on the circumferential fluid velocity and hence, on the inlet swirl, is the coefficient which tends to drive the rotor unstable. Extracted cross coupled stiffnesses were all within the bandwidth of estimated measurement error, even with some inlet swirl variations. The cross coupled stiffness decreases with increasing ratios of Re_a to Re_c, as the time used to pass through the seal becomes relatively shorter, and the fluid can not be accelerated in the circumferential direction to the same extent as with lower Re ratios.

The direct damping acts as the braking part, opposing the coupled stiffness and trying to stabilize the rotor. Direct damping depends very strongly on the Re ratio, and scatter lies well within the estimated relative error. Cross coupled damping is very small, scatter is considerable and c_c* is essentially zero.

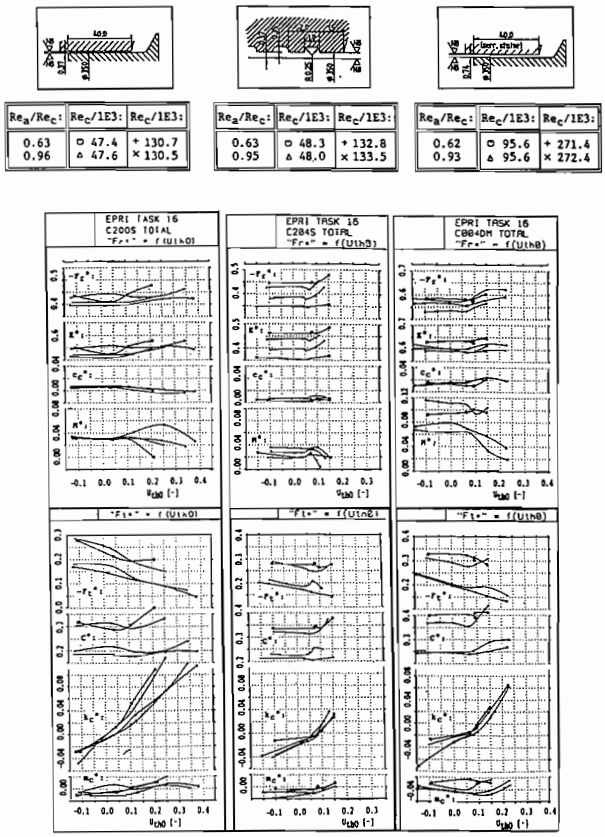

Figure 8. Overview of Measured Rotordynamic Coefficients.

The direct mass term exists at lowest Re ratios, but the relative scatter is considerable and larger than estimated errors. A distinct decrease can be found for increasing Re ratios. Averaged cross coupled mass coefficients are practically non-existent for short seals.

At the chosen whirl frequency ratio of 0.8 (vibration to running frequency), the radial and tangential forces exhibit constant averaged values at individual Re ratios. The centering radial forces do not depend on the Re ratios and the tangential forces are braking, though to a lesser extent for higher Re ratios. The cross coupled stiffness can be linearly extrapolated with the inlet swirl, including a parallel offset towards positive inlet swirls, see Figure 7. The numeric values of slopes and offsets for individual configurations and Re ratios can be found in Table 1. Extrapolation to an $U_{th0} = 0.75$ causes all tangential forces to become driving and diminishing in absolute magnitude with increasing Re ratios, see Table 2. The fact that all extrapolated F_t* values include much larger errors, i.e., approximately ± 30 percent, than estimated for measured values must be stressed.

04S

Comparison of the serrated seal with the smooth seal indicates almost no drop of the total averaged dimensionless direct stiffness. The cross coupled stiffness is reduced considerably in comparison to the values for the smooth seal, yet direct damping terms are a little higher than the values of the smooth seal. With the present moderate inlet swirl, the combination of this more advantageous combination of coefficients leads to a gain in braking forces at around 20 percent for the serrated seal. The extrapolation shown in Tables 1 and 2 indicates clearly driving (destabilizing) tendencies at realistic inlet swirls for both smooth and serrated seals. However, the serrated seal is much less destabilizing at low Re ratios, although this advantage is reduced at higher Re ratios.

Table 1. Extrapolation for k_r, F_t* and critical frequency ratio*

Note: all values concerning k_c* are extrapolated!

$$k_c^* = (U_{th0} - x_0) \cdot m$$

$$F_t^* = k_c^* - \text{OMEGA/omega} \cdot C^*$$

Critical Whirl Ratio for $F_t^* = 0$ (change from braking to driving):

$$(\text{OMEGA/omega})_c = WR_c = (U_{th0} - x_0) \cdot m / C^* = a \cdot U_{th0} - b$$

Test Series	Re-ratio: [Re_a/Re_c]	x_o [U_{th0}]	m [k_c^*/U_{th0}]	C* [–]	a [–]	b [–]	WR_c U_{th0} = .75
00S-V[1]	0.32*)	0.0	1.04	0.59	1.76	0.00	1.32
	0.63	0.025	0.59	0.35	1.69	0.04	1.23
	0.94	0.05	0.38	0.21	1.81	0.09	1.26
04S-V[2]	0.32*)	0.06	0.87	0.60	1.45	0.085	1.00
	0.63	0.075	0.61	0.36	1.69	0.125	1.14
	0.92	0.09	0.44	0.24	1.83	0.165	1.21
04D-V[3]	0.32*)	0.07	1.04	0.84	1.24	0.085	0.85
	0.61	0.095	0.57	0.40	1.42	0.135	0.93
	0.92	0.12	0.48	0.27	1.78	0.125	1.12

*)roughly estimated (from individual measurement points)

[1])00S smooth seal

[2])04S serrated seal

[3])04D serrated, double clearance seal

Table 2. Summary of F_r and Extrapolated F_t**

[U_{tho} = 0.75 frequency ratio 0.8]

(F_r* < 0: centering, F_r* > 0: decentering)

(F_t* < 0: braking, F_t* > 0: driving)

Test Series:	Fr*:			Ft*:			Re-ratio:		
	a	b	c	a	b	c	a	b	c
00S-V[1]	–0.45	–0.46	–0.44	+0.31	+0.15	+0.10	0.32	0.63	0.94
04S-V[2]	–0.45	–0.43	–0.40	+0.12	+0.12	+0.10	0.32	0.63	0.92
04D-V[3]	–0.63	–0.57	–0.59	+0.04	+0.05	+0.09	0.31	0.62	0.93

These findings imply that the use of seals with shallow serrations instead of smooth seals will slightly lower critical speeds of a pump rotor, while the most important machine damping characteristics will be improved.

04D-M

For the double clearance, "worn" serrated seal the serration depth is reduced from "new" condition in order to simulate wear, which occurs on both, rotor and stator.

The direct stiffness is not quite inversely proportional to the seal clearance, as the definition of nondimensional coefficients would suggest, resulting in higher normalized values for the worn condition.

The cross coupled stiffness is approximately inversely proportional to the seal clearance. The averages of the single and double clearance seals are not exactly equal, but scatter of the double clearance seal is notably large at the lowest force levels, and the average of the single clearance seal fits well enough into this band of standard deviations. Yet, the drop of cross coupled stiffness with increasing Re ratios is slightly larger for the double clearance seal.

Nondimensional direct damping at low Re ratio is much higher for the "worn" seal. As damping of the double clearance seal drops more extensively with Re ratios, the respective damping values match better at higher Re ratios. The nondimensional mass is approximately twice as large as for the single clearance seal; i.e., the mass becomes more significant for the resulting radial force.

In spite of the somewhat larger normalized radial force, the overall effects of wear result in the actual *dimensional* radial force to be approximately halved compared with the "new" state, as the clearance is doubled; additionally, the pressure differential becomes smaller. The nondimensional tangential force becomes distinctively higher for the double clearance at lowest Re ratios, caused by the high direct damping. At medium and high Re ratios, there is no gain in the tangential force. Accordingly, this yields dimensional forces at or below half of the values of the "new" state. Values extrapolated to higher inlet swirls are shown in Table 2. Driving normalized tangential forces are smaller for the "worn" seal than for the "new" seal. However, the advantage of the "worn" seal being less destabilizing than the "new" seal diminishes with increasing inlet swirl and increasing Re ratio.

Note that F_{t*} of the "worn" seal is approximately one order of magnitude smaller than its two components, and that the cross coupled stiffness is quite uncertain because of the extrapolation. This implies the possibility of a large relative error for F_{t*}.

Well designed swirl breaks cut the inlet swirl to approximately $U_{th0} = 0.4$, and the inlet swirl at interstage bushings is inherently zero. Hence, seal conditions become stabilizing. However, the stabilizing effect of the worn seal will be considerably smaller than the one of the new seal, as the lower pressure drop and the double clearance will result in an approximately 60 percent smaller dimensional force. Therefore, the loss of the strong damping capabilities with the wear of interstage bushings, mainly leads to the deteriorating rotor vibrational behavior. The less dramatic decrease of the critical speed due to lower seal stiffnesses is normally only of secondary importance.

Flow Resistance (Figure 9)

Some average values, mainly at low Re ratio, may not be representative for the friction behavior, indicated by the large standard deviations. This is not measurement scatter, but the change of the friction factor with Reynolds numbers, which is larger for Lambda values than for rotordynamic coefficients. However, to get a general overview, and compare individual configurations, these charts are very useful. They are comparable to each other, as the individual re-ranges measured for the three seal configurations are approximately equal and because Lambda values are about constant.

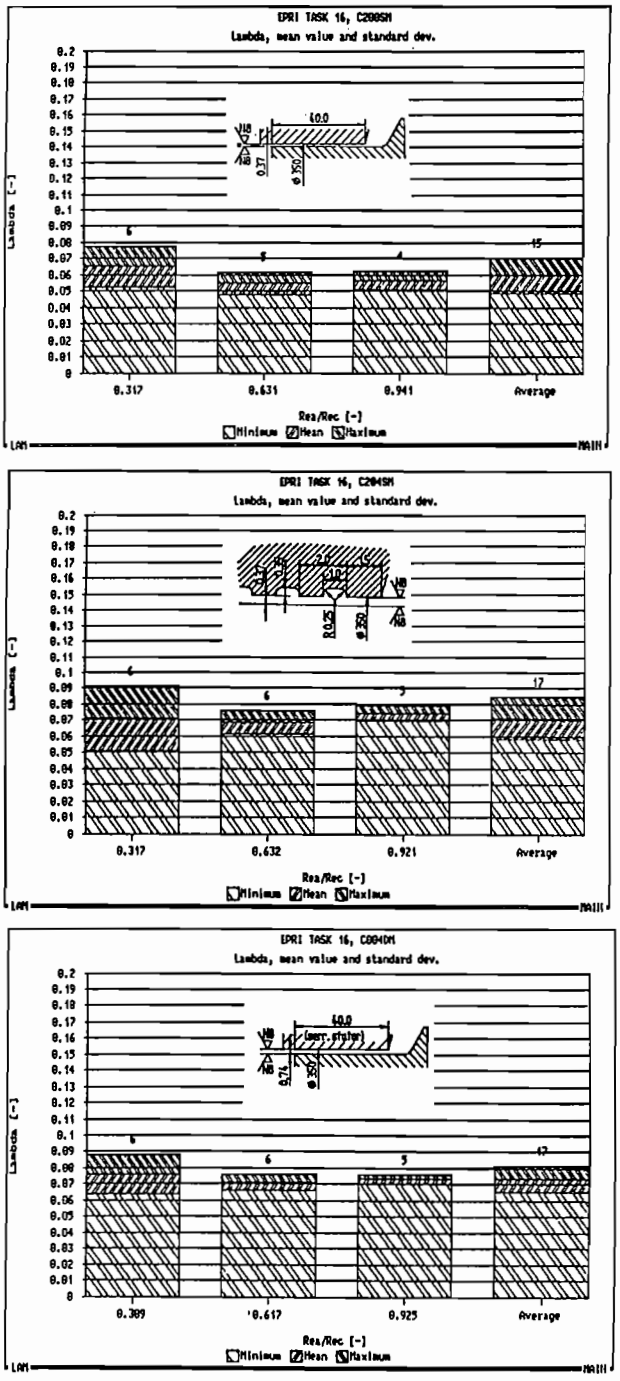

Figure 9. Overview of Measured Flow Resistances.

A high surface roughness of N8 yields quite large friction factors; the equivalent relative roughnesses is found to be around 0.02 from the comparison of the smooth seal with the Moody diagram. Indeed, comparison with other measurements reported by Florjancic and Frei [5], prove the growth of friction factors from N6 to N8 surfaces to be considerable.

Comparison of the serrated seal with the smooth seal shows that there is some gain in friction factors at low Reynolds number, and a definite increase of Lambda values is attained at higher Re-numbers. For high Re-numbers, the increase is considerable at around 30 percent. From a hydraulic point of view, a high surface roughness is desirable, even with serrated seals, to improve pump efficiency. The serration geometry might be further optimized to yield higher friction. However, further gains in friction must be compared to the changes in rotordynamic behavior.

Wear of the serrated seal, as it is simulated with test series 04D, indicates, that friction factors rise marginally when opening up the clearance to twice its original value, and the serration depth is reduced. However, even for a slightly increased Lambda value, the leakage flow does increase quite drastically with larger seal clearances; hence, pump efficiency drops.

PHYSICAL CONSIDERATIONS

A typical pressure distribution within a seal annulus caused by an eccentric position of the rotor due to shaft vibrations is shown in Figure 10. The narrow side of the annulus has a higher relative roughness inducing a higher friction factor, which results in a steeper pressure gradient and a lower axial flow velocity than encountered on the wide side. This lower axial flow on the narrow side is also responsible for the lower pressure drop at the seal entrance and the smaller pressure recovery (if existent) at the exit, with pressure loss and recovery coefficients assumed to be constant around the circumference. The difference in static pressure between the narrow and the wide side of the seal along the annulus is indicated on the left hand side of Figure 10. Integrating this difference results in the strictly radial centering force that was found first by Lomakin [12].

Similar to a journal bearing, the driving friction forces of the rotating seal part induce a circumferential flow which interacts with the asymmetric pressure distribution. This results in the maximum pressure not being at the same location as the maximum eccentricity, as shown on the right hand side of Figure 10. Integration of the pressure along and around the seal annulus yields not only a radial but also a tangential force, both depending on the vibration frequency of the rotor.

Theories

A detailed literature overview about the development of theories covering the rotordynamic effect of annular seals can be found in [19]. Summarizing briefly, Lomakin [12] started around 1958 with theoretical investigations which were carried on some ten years later by Black [13], and which were later also picked up by Childs [14] whose state-of-the-art theory was refined by Nordmann, et al. [15]. Common to all those theories is the use of bulk flow, i.e., constant velocities and pressure profiles across the seal clearance (Figure 11). Further, they use a perturbation method to calculate the vibration frequency dependent pressure and flow distribution within the seal annulus. The perturbation introduces a small circular vibration orbit of the rotor center at an arbitrary excitation frequency into the mathematical equations. The vibration induced nonuniform pressure distribution is then integrated around and along the seal to yield the same frequency dependent radial and tangential forces as the measurement.

Though theories from several authors [12, 13, 14, 15] became more and more sophisticated, even the best of them could only introduce serrations as an integral "smeared" effect. Additionally, while comparison to measured results was generally acceptable for smooth seals, serrated seals could not be predicted very well.

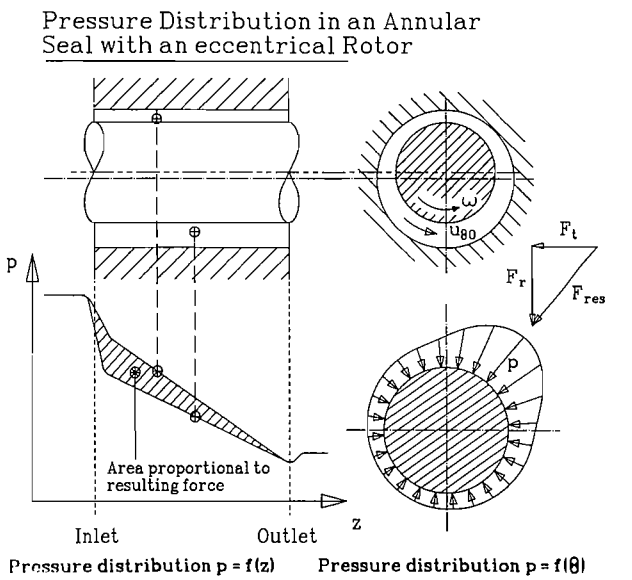

$$F_r(\Omega) = (D/2) * \int_0^L \int_0^{2\pi} p * \cos\Theta \, d\Theta \, dz$$

$$F_t(\Omega) = (D/2) * \int_0^L \int_0^{2\pi} p * \sin\Theta \, d\Theta \, dz$$

$$F_r/e = -K - c*\Omega + M*\Omega^2$$

$$F_t/e = k - C*\Omega - m*\Omega^2$$

Ω : Angular frequency of excitation
ω : Angular frequency of rotor
$u_{\theta 0}$: Corotation of the fluid

F_{res} : Resulting force
F_t : Driving force
F_r : Centering force

Figure 10. Typical Pressure Distribution in an Annular Seal.

Dietzen [16] tried a finite difference method, solving momentum and continuity equations within a serrated seal numerically, according to Navier-Stokes equations, using known turbulence models. However, this advanced tool has the distinct disadvantage that the calculation of an industrial type of serrated seal needs several hours of CPU time on an average mainframe computer and that the number of serrations is quite restricted.

Therefore, it was felt that a new theory was needed which would be more accurate than the previous standard ones [14, 15], but still would not need more than a couple of minutes of computer time. Based on the idea of a two volume theory by

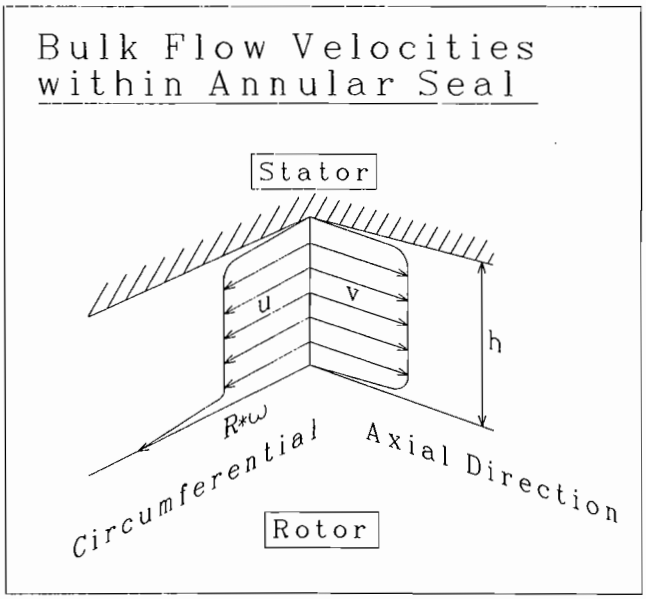

Figure 11. Principle of Bulk Flow Velocities.

Wyssmann [17] and some additional input from the theory of Scharrer [18], both for compressor labyrinths, a full three volume theory for serrated pump annular seals was set up as described in full detail by Florjancic [10]. This theory takes land parts, parts below serrations, and parts within serrations separately into account, an idea that was soon adapted by others for compressible flow labyrinth seals [19].

This discretization (Figure 12), allowed for a more detailed description of the effects within and between individual regions. Wall friction and the friction within the jet, that forms between the parts below and within a serration, can be defined by two separate laws. Though the mean axial velocity within the serration must be zero, there may still exist a vortex, which is described by an empirical factor, relating the vortex velocity to the mean axial velocity below the serration (Figure 13).

In addition to the pressure loss coefficient at the seal entrance, a pressure loss coefficient at the entrance to every subsequent land part is introduced. The additional coefficient accounts for the flow which hits the downstream wall of the preceding serration (Figure 13). The theory also allows for the new feature of pressure recovery at the seal exit, assuming that a fraction of the total velocity head is recovered when entering the downstream sump.

The differential equations defined to describe velocity and pressure distribution can not be solved analytically, and numerical methods must be applied. Splitting the seal into individual control volume areas prevents direct solution, and an iterating procedure must be developed. The velocities, the pressure and the seal clearance in all governing momentum, continuity, and shear-stress equations are perturbed with the relative eccentricity of a circular orbit (compare Figure 10).

The pressure distribution along and around the rotor surface as a function of the vibration frequency omega is found by repeating the procedure for several individual orbit frequencies. Integration of the pressure on the rotor needs to be done for the perturbed solution only, as the rotational symmetry of the centered pressure distribution yields no resulting lateral forces. The integration leads to the frequency dependent radial (F_r) and tangential (F_t) forces, which are curve fitted to yield rotordynamic coefficients.

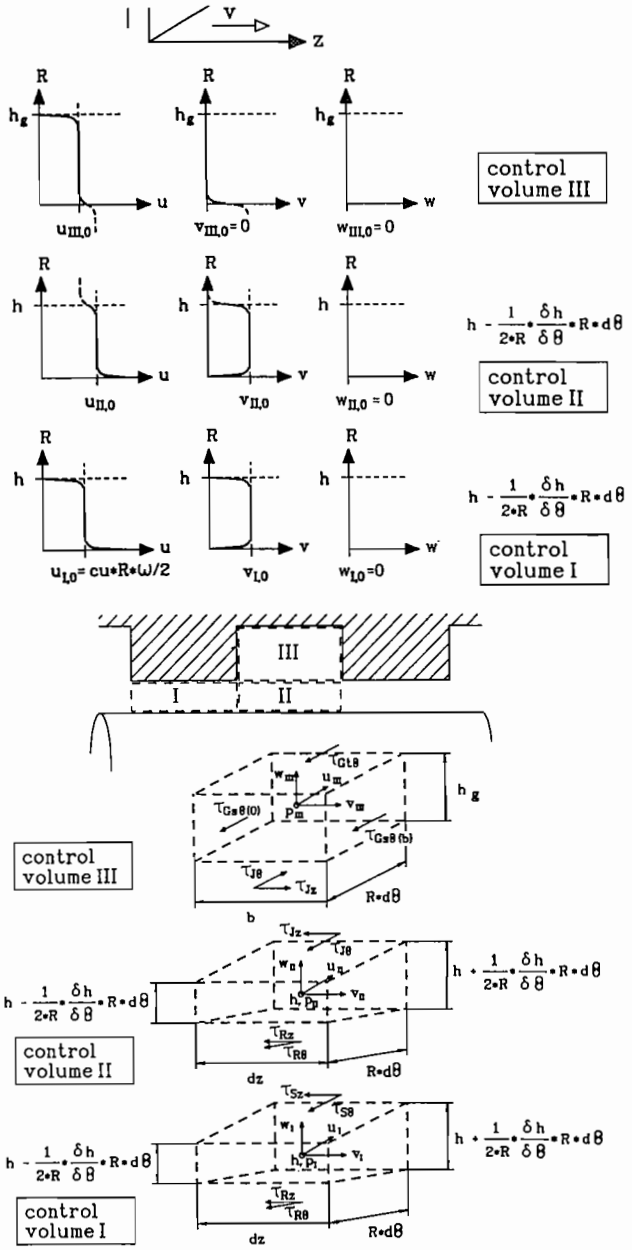

Figure 12. General Description of the New Three Volume Model and the According Bulk Flow Velocity Distribution.

Advantages of New Theory

By splitting the seal into three different sections, the flow can be described in much more detail. The three volume theory introduces an inlet loss to each land part, which is not speed dependent, and, by adapting the vortex ratio within the serration, an additional parameter is obtained, which affects the flow resistance almost independently of the circumferential velocity.

The assumption of one stable vortex within the serration needs to be introduced as a mental model only, as flow and pressure distribution within the serration are not needed. Whether there exists one vortex or a combination of several vortices, or even no vortex at all, does not affect the main model directly, but only the parameters describing the friction within the jet interface.

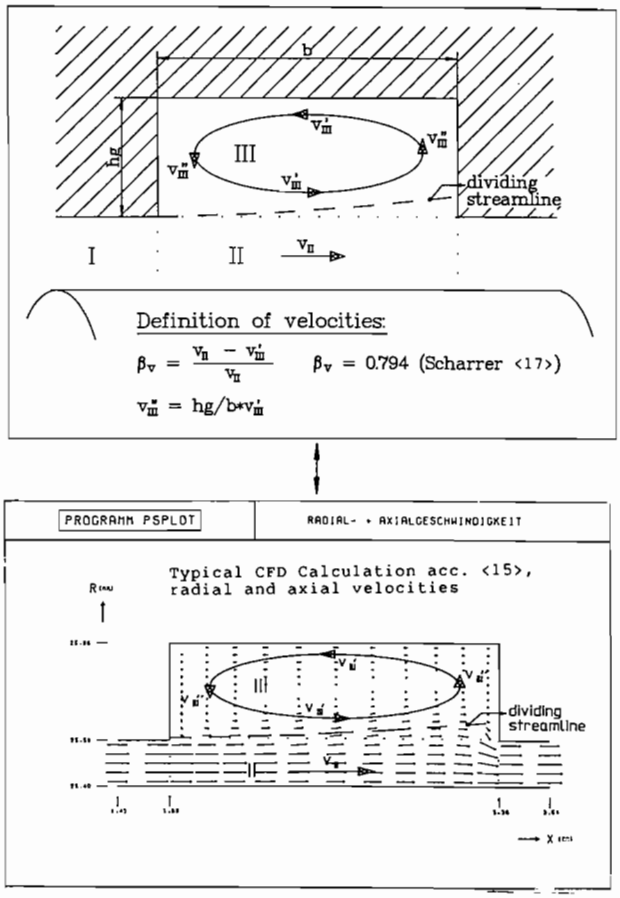

Figure 13. Vortex Velocities in a Groove, CFD Calculations Vs *New Three Volume Model.*

The main purpose of dividing into three individual areas is to allow for the more detailed flow and pressure distribution in volumes I and II. To achieve this goal, the special interface between volumes II and III is introduced, allowing for a better, intermittent type of flow friction along the stator surface. Hence, the three volume theory gives the most important additional possibility, to model the friction at the stator more accurately.

Moreover, the discrete pressure loss coefficient at the entrance to each subsequent land part within the seal allows for an extra parameter, yielding a total equivalent friction factor for the seal which is less sensitive to circumferential Reynolds numbers.

The physical insight explains why the new model yields better results then previous theories. However, one would expect that the new empirical parameters would have to be adapted for every serration variation.

The extensive data measured under an EPRI research contract for eight individual seal configurations were used to calibrate empirical friction related and pressure loss parameters. Additionally, some CFD calculations were made with the code of [16] to reconfirm the parameters found from measurement. This extensive calibration indicated that these parameters only need to be adapted for worn seals or for large changes of serration patterns. With only two sets of standard parameters for "new" and "worn" seal conditions, a wide variety of typical, rectangular serration patterns can be predicted over a broad range of Reynolds numbers without any special hydraulic input data. As a consequence, the effect of design changes and the impact of wear at annular seals on the vibrational behavior of pump rotors become predictable, providing the basis for design and maintenance rules.

COMPARISON OF THEORETICAL RESULTS WITH MEASUREMENT

Measured results were compared with the previous state-of-the-art annular seal code according to Nordmann, et al. [15], which is based on Childs [14] and the new, and more detailed, original three volume theory of Florjancic [10]. The comparison is shown in the overview of Figure 14, the upper part summarizes measured results (direct damping varies with Re ratios) for the three configurations presented previously. The lower part shows calculated results, where squares are used for the Nordmann, et al., theory [15] and diamonds for the Florjancic theory [10], "Nordmann" and "Seal" codes, respectively. While the older code overpredicts direct stiffness for the smooth seal and underestimates cross coupled stiffness and direct damping to some extent, the new three volume code predicts measured levels very closely and is able to reproduce measured tendencies quite appropriately. As measured direct mass terms are very small, relative errors for calculated results become quite large. However, predicted mass terms also reflect the low importance of these coefficients on overall rotordynamic behavior of short annular seals and prediction errors become negligible.

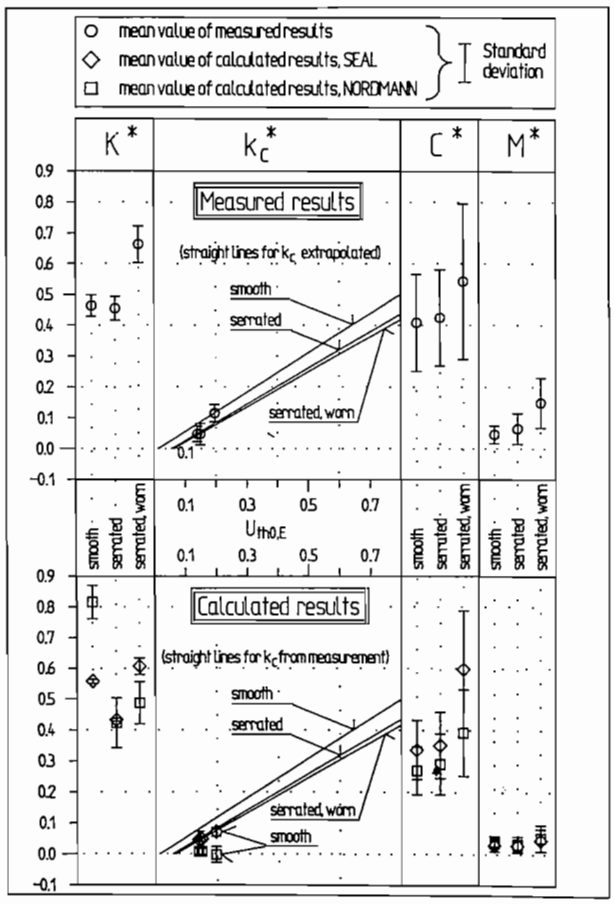

Figure 14. Comparison of Whirl Frequency Independent Rotordynamic Coefficients: Three volume theory Vs *full scale measurement.*

The overall effect of measured *vs* calculated radial and tangential forces as a function of the whirl frequency ratio (vibrational to rotational frequency) is presented in Figure 15. Here, it becomes obvious that the predicted results may be acceptable in a certain range of whirl ratios, only. Especially the Nordmann

code [15] can be seen to be restricted quite significantly, and the overall error becomes evident. However, the new "Seal" theory is quite adequate for the whole range of interest in centrifugal pumps.

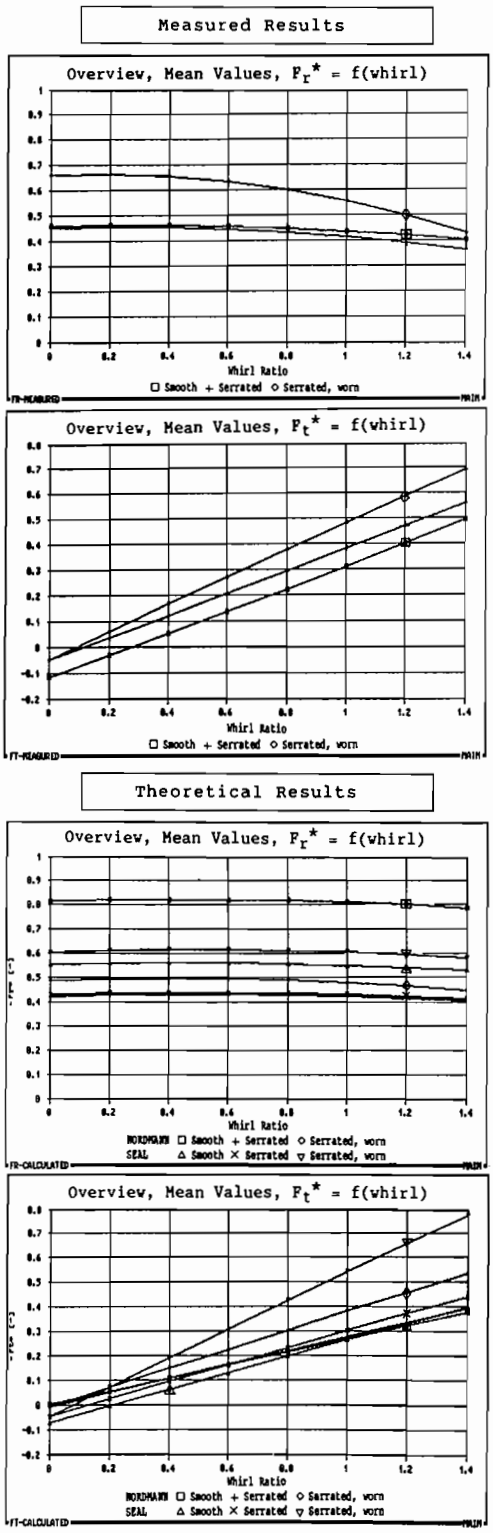

Figure 15. Comparison of Whirl Frequency Dependent Radial and Tangential Forces, Three Volume Theory Vs *Full Scale Measurement.*

Generally, previous codes as [15] were able to predict the magnitude of relevant rotordynamic coefficients, with general error levels of approximately ± 40 to 60 percent. The new three volume theory for incompressible flow, as established and calibrated by Florjancic [10], is capable of significantly improved predictions. Relative errors over the large measured range of Reynolds numbers are found to be within some ±15 to 20 percent. Hence, a powerful, yet easy to use tool for theoretical predictions of annular seals is available.

CONCLUSIONS

The importance of design and maintenance on the rotordynamic influence of annular seals in high energy centrifugal pumps, as found in various publications, has been outlined. The lack of detailed information about the effect of design parameters and wear has lead to the present extensive investigation, establishing tools to optimize seal configurations and predict their acceptable lifetime regarding wear. Rotordynamic and hydraulic seal coefficients of three typical impeller eye ring configurations have been measured at high accuracy under operating conditions of full size boiler feed pumps. A smooth seal and a serrated seal, at new and worn conditions, have been successfully investigated, and the effect of surface roughnesses on friction factors has been discussed. Normalization and type of presentation for rotordynamic coefficients have proven to be adequate, resulting in constant values over the Reynolds range measured.

The investigation revealed, that from the general coefficients used to describe the interaction at annular seals, only direct and cross coupled stiffness and direct damping are of main importance. Direct mass terms are significant only at very low ratios of axial to circumferential Reynolds numbers. Even largest mass coefficients change the radial interaction force of an annular seal only by approximately 10 percent and, hence, are of secondary importance.

In Tables 1 through 3, a rough overview of nondimensional interaction forces, including extrapolation of tangential forces, and averaged friction factors of the three configurations is given. Due to the overestimate of the seal clearance influence, double clearance values generally tend to be higher than the according single clearance values.

Damping Action

At low Reynolds number ratios, the driving tangential force is strongly influenced by individual seal configurations (Table 1). All eye ring seals which were measured result in destabilizing tangential forces at typical inlet swirls of 0.7 to 0.8. The serrated seal (04S) is clearly less destabilizing than the smooth seal (00S). As the influence of the seal surfaces on the circumferential fluid velocity reduces in proportion to the passage

Table 3. Summary of Lambda (General Overview)

Test Series:	LAMB-EFF			Re-Ratio:		
	a	b	c	a	b	c
00S-V	0.066	0.055	0.057	0.32	0.63	0.94
00S-V	0.071	0.069	0.074	0.32	0.63	0.92
04D-V [1)]	0.076	0.071	0.073	0.31	0.62	0.93

Following restrictions have to be observed, when comparing above average friction factors:

[1)]Higher Re-range at double clearance seals:
no large effect, as Lambda values of serrated double clearance seals do not vary extensively when doubling Re-numbers

time, this advantage becomes smaller with increasing Re ratios, i.e., relatively shorter fluid passage time. Properly designed large clearance seals may reduce the tangential force (04D). However, only with sufficiently small clearances, can the interstage bushings with inherently zero inlet swirl, or balance pistons and eye ring seals with swirl breaks, provide the substantial damping action needed to balance the destabilizing forces of other exciting sources, i.e., mainly impeller interaction. As this seal damping capability deteriorates with wear, leading the pump gradually towards instability, the importance of proper maintenance and replacement of worn seals becomes obvious.

Stiffening Action

For individual seal designs, the relative changes of radial forces are generally lower than of tangential forces (Table 1). It is remarkable that for a serrated seal, the loss in the stiffening effect is not large. The higher normalized radial forces of the double clearance seal indicate that dimensional centering forces will be more than half the magnitude of single clearance seals. The stiffening effect of short annular seals is small compared to journal bearing stiffnesses or to the mechanical stiffness of a rotor with few stages. Only long seals, i.e., balance pistons and throttling bushes, introduce high stiffness. The stiffness of short seals becomes more important on pumps with a large number of stages. The overall stiffening effect of seals and its reduction with wear is usually less dramatic than the damping influence; yet, it is not negligible. Generally, critical speeds are lowered to some extent with the decreased stiffness of worn seals and may fall into the operating range, inducing higher vibrations. Again, the significance of maintenance, replacing worn seals in time and preventing premature wear, becomes apparent.

Flow Resistance

Generally, friction factors of smooth surfaces vary considerably in the Re-range (20,000 ÷ 260,000). However, for the present large relative roughnesses (approximately 0.02, comparing to Moody's diagram), Lambda coefficients become almost constant at moderate Reynolds numbers.

As has been found by comparison with data from earlier measurement, quadrupling the surface roughness to the actual N8, results in a distinct rise in flow resistance and, hence, in an upgraded pump efficiency. Compared to the smooth seal, the measured serrated seal (04S) exhibits an increase in flow resistance with increasing Re-numbers. Simulated wear reveals slightly higher friction factors at the resultant higher flows. However, better hydraulic performance could certainly be attained, e.g., by a deeper serration and shorter land portions. Yet, this advantage might be quickly reduced, as the remaining land portions tend to be worn off sooner. Additionally, such a hydraulically optimized serration pattern is detrimental to rotordynamic behavior because of the larger serration depth ("anti-Lomakin" seal).

Final Remarks

The comparison of rotordynamic and hydraulic coefficients of smooth *vs* serrated seals showed that configurations with advantages in one respect may have disadvantages in other respects. The choice of an appropriate seal configuration depends on the application of the pump, i.e., on whether hydraulic or rotordynamic behavior is more critical [6]. Rotordynamic behavior in a high energy pump like a boiler feed pump may not be optimum when using deeply serrated antistiffness seals in order to gain increased efficiencies.

After the right choice of a configuration by the designer, annular seals of high energy centrifugal pumps also need to be maintained properly. Premature wear by highly abrasive media or by rub should be avoided, and the worn seal must be replaced in time to avoid excessive loss of damping and, as a consequence, vibration induced malfunction or even catastrophic failure.

NOMENCLATURE

C	[Ns/m]	symmetric direct damping coefficient
c	[m/s]	total velocity
c_c	[Ns/m]	skew-symmetric cross-coupled damping coefficient
D_2	[m]	outer diameter of impeller
dp	[N/m²]	total pressure differential across seal
e	[m]	eccentricity
F_r	[N]	force in radial direction
F_t	[N]	force in tangential direction
F_x	[N]	force in x-direction
F_y	[N]	force in y-direction
h_0	[m]	mean seal gap width
K	[N/m]	symmetric direct stiffness coefficient
k_c	[N/m]	skew-symmetric cross-coupled stiffness coefficient
Lambda	[-]	Friction coefficient, where $dp = 0.5 \cdot rho \cdot v^2 \cdot ([Lambda \cdot L_{Seal}]/(2h_0) + Ze_i = Ze_o]$
L_{Seal}	[m]	seal length
M	[kg]	symmetric direct mass coefficient
m_c	[kg]	skew-symmetric cross coupled mass coefficient
nue	[m²/s]	kinematic viscosity
OMEGA	[rad/s]	angular frequency of excitation
omega	[rad/s]	angular frequency of rotor
R	[m]	seal radius
Re_a	[-]	axial Reynolds number, $Re_a = v \cdot 2 \cdot h_0/nue$
Re_c	[-]	circumferential Reynolds number, $Re_c = R \cdot omega \cdot 2 \cdot h_0/nue$
rho	[kg/m³]	density
u	[m/s]	circumferential velocity
U_{th0}	[-]	dimensionless circumferential velocity, $U_{th0} = u/(R \cdot omega)$
v	[m/s]	axial velocity
X	[m]	measured horizontal displacement
Y	[m]	measured vertical displacement
Ze_i	[-]	pressure loss coefficient at inlet of seal
Ze_o	[-]	pressure loss coefficient at outlet of seal

Superscripts:

*	dimensionless value

Subscripts:

i	inlet
o	outlet

REFERENCES

1. Pace, S. E., Florjancic, S., and Bolleter, U., "Rotordynamic Developments for High Speed Multistage Pumps," Proceedings of the Third International Pump Symposium, Turbomachinery Laboratory, Department of Mechanical Engineering, Texas A&M University, College Station, Texas (1986).
2. France, D., "Rotor Instability in Centrifugal Pumps," The Shock and Vibration Digest, *18* (1) (1986).

3. Verhoeven J., "Rotordynamic Considerations in the Design of High Speed Centrifugal Pumps," Proceedings of the Fifth International Pump Users Symposium, Turbomachinery Laboratory, Department of Mechanical Engineering, Texas A&M University, College Station, Texas (1988).

4. Valantas R. A., and Bolleter, U., "Solutions to Abrasive Wear-Related Rotordynamic Instability Problems on Prudhoe Bay Injection Pumps," Proceedings of the Fifth International Pump Users Symposium, Turbomachinery Laboratory, Department of Mechanical Engineering, Texas A&M University, College Station, Texas (1988).

5. Florjancic, S., and Frei, A., "Dichtspaltströmung in Pumpen: Bedeutung für die Rotordynamik und theoretische Betrachtungen," Proceedings of the Pumpentagung Karlsruhe (October 1988).

6. Florjancic, D., and Florjancic, S., "Hydraulic and Rotordynamic Influence on the Choice of Different Pump Types," Proceedings of the Conference on Hydraulic Machinery 88, Ljubljana (1988).

7. Jery, B., Acosta, A. J., Brennen, C. E., and Caughey, T. H., "Hydrodynamic Impeller Stiffness, Damping and Inertia in the Rotordynamics of Centrifugal Flow Pumps," Third Workshop on Rotor Instability Problems in High Performance Turbomachinery, Turbomachinery Laboratory, Texas A&M University, College Station, Texas (1984).

8. Bolleter, U., and Wyss, A., "Measurement of Hydrodynamic Interaction Matrices of Boiler Feed Pump Impellers," Journal of Vibration, Stress and Reliability in Design, 109, pp. 144-151 (April 1987).

9. Bolleter, U., Leibundgut, E., and Stürchler, R., "Hydraulic Interaction and Excitation Forces of High Head Pump Impellers," Proceedings of the 3rd Joint ASCE/ASME Mechanics Conference: Pumping Machinery Symposium, San Diego, California (July 1989).

10. Florjancic, S., "Annular Seals of High Energy Centrifugal Pumps: A New Theory and Full Scale Measurement of Rotordynamic Coefficients and Hydraulic Friction Factors," Ph.D. Thesis, Federal Institute of Technology (ETH) Zürich, Switzerland Nr. 9087 (May 1990).

11. Florjancic, S., "Annular Seals of High Energy Centrifugal Pumps: Presentation of Full Scale Measurement," Proceedings of the 6th Workshop on Rotordynamic Instability Problems, Turbomachinery Laboratory, Texas A&M University (May 1990).

12. Lomakin, A. A., "Calculating the Critical Speed and the Conditions to Ensure Dynamic Stability of the Rotors in High Pressure Hydraulic Machines, Taking Account of the Forces in the Seals," Energomashinostroenie, 4 (4), pp. 1-5 (April 1958).

13. Black, H. F., "Effects of Hydraulic Forces in Annular Pressure Seals on the Vibrations of Centrifugal Pump Rotors," Journal of Mechanical Engineering Science, 11 (2) (1969).

14. Childs, D. W., "Finite Length Solution for Rotordynamic Coefficients of Turbulent Annular Seals," ASME Transaction Journal of Lubrication Technology, 105, pp. 437-444 (July 1983).

15. Nordmann, R., Dietzen, F. J., Janson, W., Frei, A., and Florjancic, S., "Rotordynamic Coefficients and Leakage Flow for Smooth and Grooved Seals in Turbopumps," Proceedings of the International Conference on Rotordynamics, JSME, IFToMM, Tokyo, Japan, pp. 619-627 (September 1986).

16. Dietzen, F. J., and Nordmann, R., "Calculating Rotordynamic Coefficients of Seals by 'Finite-Difference' Techniques," Fourth Workshop on Rotordynamic Instability Problems in High Performance Turbomachinery, Turbomachinery Laboratory, Texas A&M University (June 1986).

17. Wyssmann, H. R., Pham, T. C., and Jenny, R. J., "Prediction of Stiffness and Damping Coefficients for Centrifugal Compressor Labyrinth Seals," ASME 84-GT-86 (1984).

18. Scharrer, J. K., "A Comparison of Experimental and Theoretical Results for Labyrinth Gas Seals," TRC-SEAL-3-87, Turbomachinery Laboratory, Texas A&M University (1987).

19. Weiser, H. P., "Ein Beitrag zur Berechnung der dynamischen Koeffizienten von Labyrinthdichtungssystemen bei turbulenter Durchströmung mit kompressiblen Medien," Ph.D. Thesis, University of Kaiserslautern, W-Germany, D 386 (November 1989).

BIBLIOGRAPHY

Glienicke, J., "Experimentelle Ermittlung der statischen und dynamischen Eigenschaften von Gleitlagern für schnellaufende Wellen," Forschungsberichte VDI-Z Reihe 1, 22 (1970).

Lund, J. E., and Thompson, K. K., "A Calculation Method and Data for the Dynamic Coefficients of Oil-lubricated Journal Bearings: Topics in Fluid Film Bearing and Rotor Bearing System Design and Optimization," ASME, p. 1 (1978).

ACKNOWLEDGEMENTS

All geometries, including some further variants, have been measured under EPRI (Electric Power Research Institute, Incorporated, Palo Alto California) contract RP 1884-10 at Sulzer Brothers, Winterthur, Switzerland. The authors wish to thank EPRI and Sulzer Brothers for the kind permission to publish the presented data.